Inorganic Chemistry Research

Article

Functionalization of Mesoporous CuS@mSiO$_2$ Core-Shell Nanoparticles by Cu(II) and Ni(II) Schiff Base Complexes: Synthesis, Characterization, Antibacterial Activity, Antibiotic Loading, DNA Cleavage and Enzyme Immobilization

Ameneh Ahmadi[a], Tahereh Sedaghat[a,*] and Hossein Motamedi[b,c]

[a]*Department of Chemistry, Faculty of Science, Shahid Chamran University of Ahvaz, Ahvaz, Iran*
[b]*Department of Biology, Faculty of Science, Shahid Chamran University of Ahvaz, Ahvaz, Iran*
[c]*Biotechnology and Biological Science Research Center, Shahid Chamran University of Ahvaz, Ahvaz, Iran*

Received: September 17, 2022; Accepted: October 25, 2022
Cite This: *Inorg. Chem. Res.* **2022**, *6*, 98-106. DOI: 10.22036/icr.2022.362554.1135

Abstract: 3-Chloropropyltrimethoxysilane (CPTMS) was grafted on the surface of mesoporous CuS@mSiO$_2$ core-shell nanoparticles and then condensed with a tetradentate Schiff base, bis(salicylaldehyde)diethylenetriamine (H$_2$Saldien), to obtain CuS@mSiO$_2$-SB. The latter material was treated with Cu(II) or Ni(II) acetate salts and therefore metal Schiff base complexes were immobilized on mesoporous nanocomposites, CuS@mSiO$_2$-SB-Cu and CuS@mSiO$_2$-SB-Ni. The characterization of synthesized nanomaterials was carried out by Fourier-transform infrared spectroscopy (FT-IR), energy dispersive X-ray analysis (EDX), field emission scanning electron microscope (FESEM), transmission electron microscopy (TEM), low angle X-Ray diffraction (LA-XRD), Brunauer–Emmett–Teller (BET) surface area analysis, and thermogravimetric analysis (TGA). The results confirm a core-shell mesoporous structure for nanocomposites and prove the presence of all elements. Nanoparticles have spherical morphology with a mean diameter less than 100 nm. The synthesized nanocomposites were evaluated for antibacterial activity against Gram-positive (*S. aureus*) and Gram-negative (*P. aeruginosa*) bacteria and as carrier for streptomycin, gentamycin and polymyxin. The DNA cleavage activity of nanoparticles was also studied by agarose gel electrophoresis method. Nanocomposites were found to be good carrier for antibiotic, significantly inhibit bacterial growth and completely degrade the treated DNA. Also nanoparticles efficiently immobilized α-amylase enzyme.

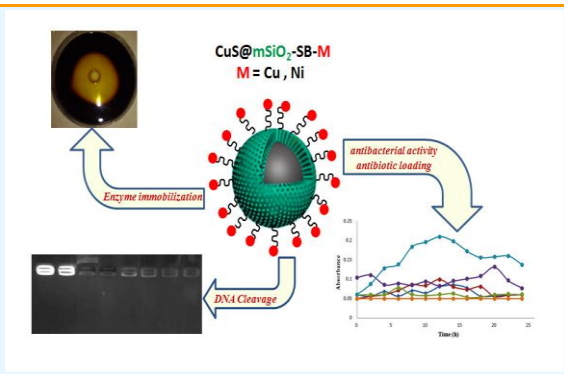

Keywords: Mesoporous, Schiff Base, Core-Shell, Nanoparticles

1. INTRODUCTION

In the last decade, scientists have discovered, developed and used various types of porous materials including metal-organic frameworks (MOFs), covalent organic frameworks (COFs), zeolitic materials and porous silica, carbon and metals.[1-8] According to the classification of IUPAC, porous materials are divided into three categories: microporous (pore diameters less than 2 nm), mesoporous (pore diameters between 2-50 nm) and macroporous (pore diameters greater than 50 nm).[9] Mesoporous silica materials have attracted a lot of attention by chemists and pharmacists due to their various features such as high surface area, uniform pore channels, facile synthetic method, stability, biocompatibility, and easy functionalization due to active silanol groups.[10,11] These materials are used for adsorption, molecular sieves, catalyst supports, ion-exchangers, biomedical applications, tissue-engineering, drug delivery and for many other applications.[12,13] Silica is the most common inorganic material used for coating the surface of nanoparticles, because it improves the chemical stability of nanoparticles, provides suitable particles for biological applications, and allows easy functionalization either in-situ or post-grafting due to the presence of silanol groups.[14,15] Among the silica substrates, MCM-41 has advantages such as the adjustable and uniform pores, particle size control and high surface area and therefore it has been widely studied. The size and regularity of the pores in mesoporous silica (mSiO$_2$) make them suitable for embedding small molecules such as enzymes. These

materials have been promising supports for immobilization and stability of enzymes. Enzymes are immobilized on mesoporous silica through chemical or physical interactions. Immobilized enzymes were used for biosensing, biofuels, drug delivery and recoverable and stable heterogeneous biocatalysts.[16-18]

In the present research work, CuS@mSiO$_2$ which contains copper sulfide core and mesoporous silica shell is functionalized with a Schiff base and its copper and nickel complexes. This work is continuing of our recent researches on synthesis and application of modified mesoporous nanoparticles.[19-23] We chose CuS because of its potential to be used as a promising candidate for photothermal therapy.[24-27] These organic-inorganic hybrid nanoparticles were intended to provide efficient support for interaction with antibiotics and enzymes. Copper and nickel complexes looks suitable candidates for this propose due to low toxic, good biological activity and their application as biocatalyst centers. The antibacterial activity, streptomycin, gentamycin and polymyxin loading, α-amylase enzyme immobilization and also DNA cleavage activity of the synthesized nanocomposites were also investigated

2. EXPERIMENTAL

Materials and methods

All starting materials were purchased from Merck chemical company and used without further purification. Deionized water was obtained from Millipore pure water system.

FT-IR spectra were recorded by a BOME/MB 102 spectrophotometer within the 400–4000 cm^{-1} range using the KBr pellets. Morphology and dimensions of nanoparticles were examined using field emission scanning electron microscopy (FE-SEM) equipped with EDS analyzer model Mira 3-XMU and with an accelerating voltage of 15 kv. Transmission electron microscopy (TEM) images were obtained using a TEM LEO912-A. Powder X-ray diffraction (PXRD) patterns were collected by a PW 1730 X-ray diffractometer model X Pert Pro using CuK$_\alpha$ irradiation at 40 kv and 30 mA. N_2 adsorption-desorption isotherms were obtained at liquid N_2 temperature on a Belsorp mini II instrument. Samples were degassed at 120 °C for 15 h prior to analysis. The surface area was calculated by Brunauer-Emmet-Teller (BET) method, and pore size distribution was estimated from the adsorption branch of the isotherm by the Barrett-Joyner-Halenda (BJH) method. Thermogravimetric analysis (TGA) of the samples was performed using a TA Q600 instrument under flowing argon with a heating rate of 10 °C min^{-1}. Thermogravimetric analysis (TGA) of the prepared catalyst was performed on a STA 1500 thermal analyzer under N_2 atmosphere from 25 to 800 °C and heating rate of 10 °C min^{-1}. Bacterial growth was measured through reading the absorption of bacterial suspension by ELISA reader (Bio-Rad 680 Microplate Reader, USA) and growth curve analysis.

Synthesis of CuS nanocrystals

A solution of citrate-coated CuS nanocrystals was prepared according to the method reported earlier.[28] Anhydrous Copper (II) chloride (0.2 mmol, 0.027 g) and sodium citrate (0.136 mmol, 0.04 g) were dissolved in deionized water (180 mL), and then a solution of sodium sulfide (20 mL, 10 mmol/L) was dropwise added. This solution was stirred for 5 minutes at room temperature and during this time its color changed from light blue to dark brown.

Then the solution was heated to 90 °C and vigorously stirred for 15 min at this temperature. After this period, the system was allowed to cool down to the ambient temperature. Finally, the dark-green solution of citrate-coated CuS nanocrystals was cooled in ice-cold water bath and stored at 4 °C.

Synthesis of CuS@mSiO$_2$

CuS@mSiO$_2$ was synthesized by the procedure reported in the literature with a little modification.[28] A solution of above CuS nanocrystals (65 mL) and CTAB (0.7 g) was vigorously stirred for 2 h at 40 °C. Then a solution of NaOH (100 µL, 30 mg/mL) and ethanol (3 mL) were added, followed by TEOS (100 µL). The mixture was vigorously stirred for 1.5 h at 40 °C. The mixture was maintained in an oven at 60 °C for 24 h. The resulting blue gel was centrifuged for 10 min and washed with deionized water and ethanol. For the removal of CTAB, the product was dispersed in an ethanolic solution of NH_4NO_3 (50 mL, 10 mg/mL) with an ultrasonic bath for 30 min and then vigorously stirred for 2 h at 50 °C. The resulting CuS@mSiO$_2$ nanoparticles were centrifuged, washed with deionized water and ethanol and then dried in oven at 60 °C for 24 h.

Synthesis of 3-chloropropylsilane-functionalized CuS@mSiO$_2$ nanoparticles (CuS@mSiO$_2$-CPS)

CuS@mSiO$_2$ nanoparticles (0.1 g) were dispersed in ethanol (25 mL) for 20 min in an ultrasonic bath. Then, 1 mL of 3-chloropropyltrimethoxysilane (CPTMS) was added dropwise and the mixture was refluxed under N_2 atmosphere at 100 °C for 24 h. The product was centrifuged for 10 min, washed with ethanol and then dried in oven at 60 °C for 24 h.

Synthesis of schiff base-functionalized CuS@mSiO$_2$ nanoparticles (CuS@mSiO$_2$-SB)

For synthesis of the Schiff base, bis(salicylaldehyde)diethylenetriamine (H_2Saldien), salicylaldehyde (2 mmol, 0.21 mL) and diethylenetriamine (0.11 mL, 1 mmol) were stirred in ethanol (15 mL). A yellow solution was formed immediately. To this solution, CuS@mSiO$_2$–CPS (0.1 g) and triethylamine (0.14 mL, 1 mmol) were added and refluxed for 24 h. after this period, the mixture was centrifuged and washed several time with ethanol. CuS@mSiO$_2$-SB nanoparticles were dried in oven at 60 °C for 24 h.

Synthesis of CuS@mSiO$_2$–SB-Cu and CuS@mSiO$_2$–SB-Ni

CuS@mSiO$_2$–SB (0.1 g) was sonicated in ethanol (20 mL) for 20 min. Then, a solution of Cu(CH$_3$COOH)$_2$.H$_2$O or Ni(CH$_3$COOH)$_2$.4H$_2$O (1 mmol) in ethanol (15 mL) was added. This mixture was sonicated for 2 h at 60 °C and followed by stirring for 24 h at R.T. The product was centrifuged for 10 min, washed several time with ethanol and then dried in oven at 60 °C for 24 h.

Antibiotic loading and antibacterial activity

In order to loading of streptomycin, gentamycin and polymyxin on the nanocomposites, 20 mg of CuS@mSiO$_2$, CuS@mSiO$_2$-SB, CuS@mSiO$_2$-SB-Cu or CuS@mSiO$_2$-SB-Ni was added to 1 mL of antibiotic solution (10 mg/mL Milli-Q water). The mixture was then stirred at room temperature for 24 h and the antibiotic loaded composites were separated by centrifugation at 10000 rpm for 5 min. Also, to remove the surplus antibiotic, nanocomposites were washed with deionized water for three times. The antibacterial activity of the nanocomposites was checked against a Gram positive bacterium, *Staphylococcus aureus* and a Gram negative species, *Pseudomonas aeruginosa*. For this purpose, 20 mg of each compound in Milli-Q water (1 mL) was inoculated with Mueller-Hinton broth (Merck, Germany) containing bacterial suspension (*P. aeruginosa or S. aureus*) with 0.5 McFarland. The cultures were then incubated at 37 °C, and bacterial growth was monitored every 4 h through measuring the bacterial suspension absorbance at 655 nm using ELISA reader. Simultaneously controls including bacterial culture without nanocomposite as well as uninoculated culture medium containing nanocomposite were regarded. Minimum Inhibitory Concentration (MIC) and Minimum Bactericidal Concentration (MBC) were determined by microdilution technique using 0.5, 1, 2, 4, 8 and 16 mg/mL concentrations of composites.

Gel electrophoresis assay

Firstly, the bacterial DNA was extracted by boiling method described earlier.[29,30] Then a suspention of each compound in $CHCl_3$ (20 mg/mL) was prepared and 100 µL of it was mixed with 100 µL of DNA solution. This mixture was incubated at 37 °C for 2h. A positive control was prepared through mixing H_2O_2 (100 µL) with DNA (100 µL) and treated in the same way as before. Also, an untreated DNA was regarded as negative control. To investigate the effect of nanocomposites on DNA, agarose gel electrophoresis was performed. One percent agarose was prepared in TAE buffer and boiled. DNA safe stain was added to the gel and poured in horizontal electrophoresis tray. 5 µL of each treated DNA was mixed with 2µL of loading dye and loaded in agarose gel. A 1 Kb DNA ladder was also loaded in a well. Electrophoresis was done at 80 V for 1 h. The gel was documented under UV irradiation by UVI/TEC gel documentation.

Enzyme immobilization

CuS@mSiO$_2$, CuS@mSiO$_2$-SB, CuS@mSiO$_2$-SB-Cu or CuS@mSiO$_2$-SB-Ni (20 mg) was added to a solution of α-amylase enzyme (2 mg) in 1 mL of phosphate buffer saline (PBS). This mixture was incubated at continuous shaking (75 rpm) at 37 °C for 24 h. Then, the samples were isolated by high-speed centrifuging at 10000 rpm for 5 min and washed with PBS three times. These enzyme conjugated nanocomposites were dispersed in phosphate buffer saline (500 µL) and then sterile paper disks were saturated with this suspension. Saturated paper disks were placed on plates containing starch 10% and incubated at 37 °C for 24 h. In the following, iodine solution was added on the surface of agar and the area of inhibition around each disk was recorded as the α-amylase activity. A disk saturated with the third wash solution was considered as a control for each compound.

3. RESULTS AND DISCUSSION

Synthesis and characterization

The synthesis pathway of the CuS@mSiO$_2$-SB-M (M = Cu and Ni) nanocomposites is shown in Figure 1. CuS nanocrystals are surrounded by negatively charged hydrophilic citrate ligands in aqueous solution. Silica shell cannot be directly coated on CuS nanoparticles because silica gains a negative charge due to hydrolysis. CTAB as a cationic surfactant coats around the CuS nanocrystals and causes the charge of nanoparticles to change from negative to positive.[28] Nanocrystals surrounded by excess CTAB act as soft template. In the next step, TEOS is hydrolyzed and condensed under alkaline conditions and SiO_2 is grown around the template. After removal the CTAB, CuS@mSiO$_2$ nanoparticles was functionalized by reaction with chloropropyltrimethoxysilane (CPTMS). During this reaction, the methoxy groups of CPTMS react with the active silanol groups and MeOH is eliminated. Tetradentate Schiff base, H_2Saldien, was prepared by reaction of salicylaldehyde and diethylenetriamine in 1:2 mole ratio and this solution was reacted in situ with CuS@mSiO$_2$–CPS in the presence of Et_3N as a base. In this reaction the –NH group of H_2Saldien ligand reacts with the –Cl group on CuS@mSiO$_2$–CPS and as a result, a tetradentate ligand is immobilized on silica support. Finally, metal complexes are anchored on nanoparticles by reaction of the CuS@mSiO$_2$–CPS-SB with metal acetate salts. In this reaction, the supported Schiff base acts as a tetradentate ligand via phenolate oxygens and imine nitrogens. The synthesized organic-inorganic hybrid materials were characterized by FT-IR, EDS, FE-SEM, TEM, LA-XRD, BET and TGA techniques.

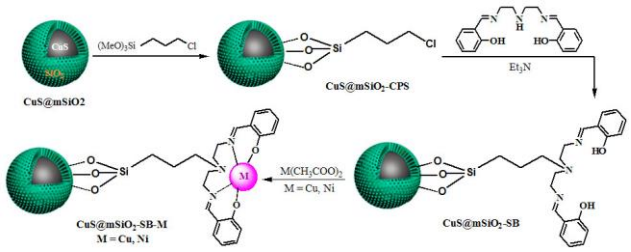

Figure 1. The route for synthesis of the CuS@mSiO$_2$-SB-M (M = Cu and Ni).

The FT-IR spectra of the CuS@mSiO$_2$-CTAB, CuS@mSiO$_2$, CuS@mSiO$_2$-CPS, CuS@mSiO$_2$-SB, CuS@mSiO$_2$-SB-Cu and CuS@mSiO$_2$-SB-Ni are shown in Figure 2. The band at about 618 cm^{-1} was assigned to Cu–S stretching vibration.[31] Asymmetric stretching, symmetric stretching and bending vibration modes of the Si–O–Si in SiO_2 are appeared at 1074, 796 and 458 cm^{-1}, respectively, in Figure 2a and with slightly shifts in other spectra.[20,23,32] In the FT-IR spectrum of CuS@mSiO$_2$-CTAB (Figure 2a), the bands at 2919 and 2850 cm^{-1}

are ascribed to the C−H stretching vibrations and at 1488 cm^{-1} to bending vibration modes of $–(–CH_2–)_3–$ group of CTAB.[20] The disappearance of these strong characteristic bands in the next spectrum confirms the removal of CTAB surfactant from the structure. The bands at 2932 and 2983 cm^{-1} in the spectrum of CuS@mSiO_2-CPS were related to $–CH_2$ alkyl vibrations of CPS. In the IR spectrum of CuS@mSiO_2-SB (Figure 2d), the presence of a band at 1641 cm^{-1} is attributed to the imine groups (C=N) of H_2Saldien and confirms that the Schiff base ligand is successfully grafted on mesoporous silica nanoparicles. In the spectra of CuS@mSiO_2-SB-Cu and CuS@mSiO_2-SB-Ni (Figure 2f and 2e), the C=N stretching band is shifted to lower frequency and appeared at 1627 and 1625 cm^{-1}, respectively. This observation proves the binding of metal to imine groups of the grafted ligand. In the all spectra, the band about 1620 cm^{-1} was related to H_2O molecules physically adsorbed by mesoporous silica and the broad band around 3400 to the O–H of silanol and water.

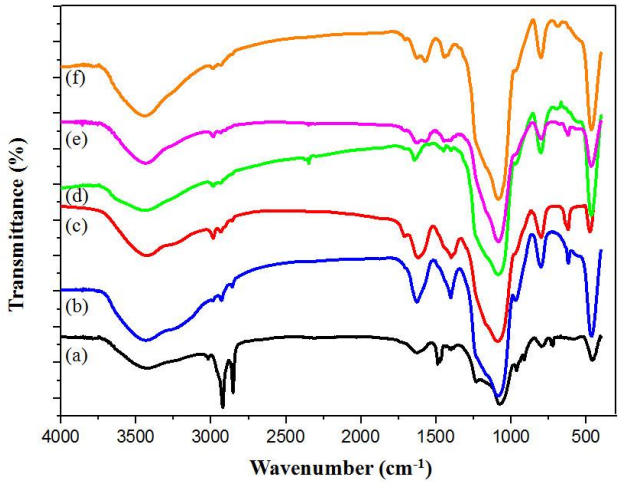

Figure 2. FT-IR spectra of synthesized nanocomposites (a) CuS@SiO_2-CTAB (b) CuS@mSiO_2 (c) CuS@mSiO_2-CPS (d) CuS@mSiO_2-SB (e) CuS@mSiO_2-SB-Cu (f) CuS@mSiO_2-SB-Ni.

Figure 3 shows the chemical composition of CuS@mSiO_2, CuS@mSiO_2-SB-Cu and CuS@mSiO_2-SB-Ni by energy dispersive X-ray spectroscopy (EDS). The presence of Si, Cu, N, C, O, S and Ni elements confirms the successful immobilization of Schiff base metal complex on the CuS@mSiO_2 nanoparticles. Figures 4 and 5 also visualize the presence and uniform distribution of elements in the specified area of CuS@mSiO_2-SB-Cu and CuS@ mSiO_2-SB-Ni, respectively, by EDX mapping. These images confirm good distribution of metal on the nanoparticles.

Figure 6 shows the FESEM images of CuS@mSiO_2, CuS@mSiO_2-SB-Cu and CuS@mSiO_2-SB-Ni nanoparticles. As shown, all samples have spherical morphology with a diameter below 100 nm and

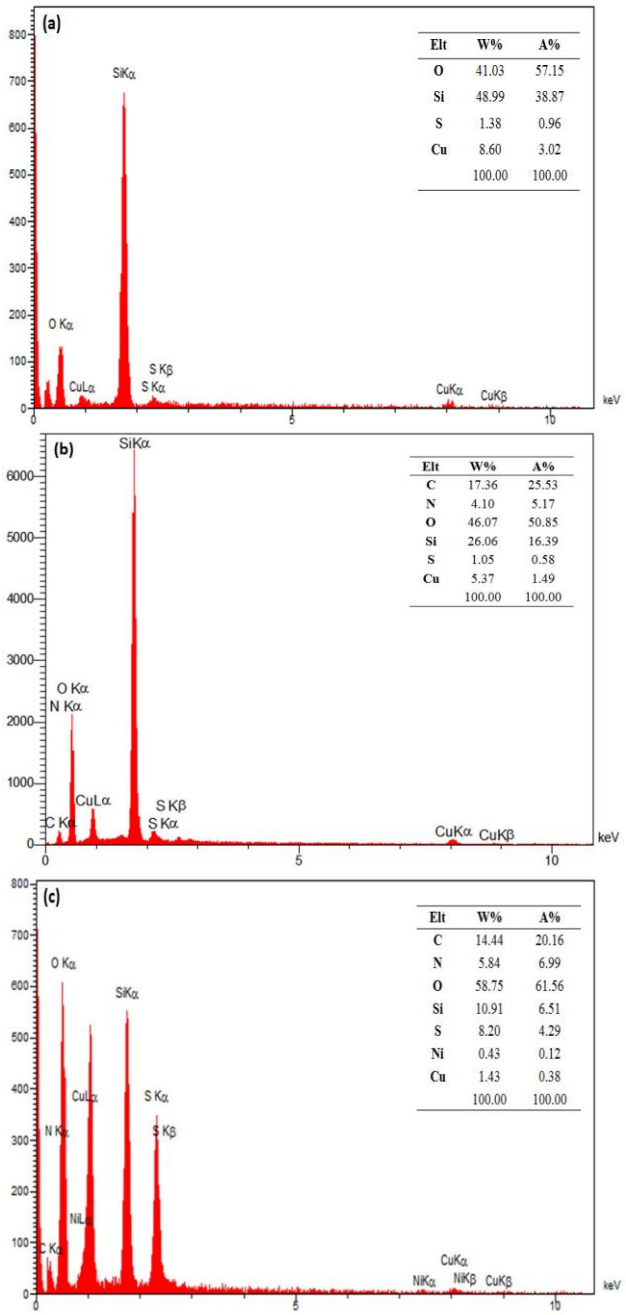

Figure 3. The Elemental composition of (a) CuS@mSiO_2, (b) CuS@mSiO_2-SB-Cu and (c) CuS@mSiO_2-SB-Ni determined by EDS analysis.

functionalization has not significantly changed the size and morphology. The TEM images of CuS@mSiO_2 and CuS@mSiO_2-SB-Ni (Figure 7) confirm a core-shell structure for nanoparticles as the CuS core are coated by SiO_2 shell. Since functionalization reduces the order of mesostructure, the TEM image of CuS@mSiO_2-SB-Ni shows changes that confirmed by XRD and BET results.

The low-angle XRD patterns of CuS@mSiO_2, CuS@mSiO_2-SB-Cu and CuS@mSiO_2-SB-Ni are shown

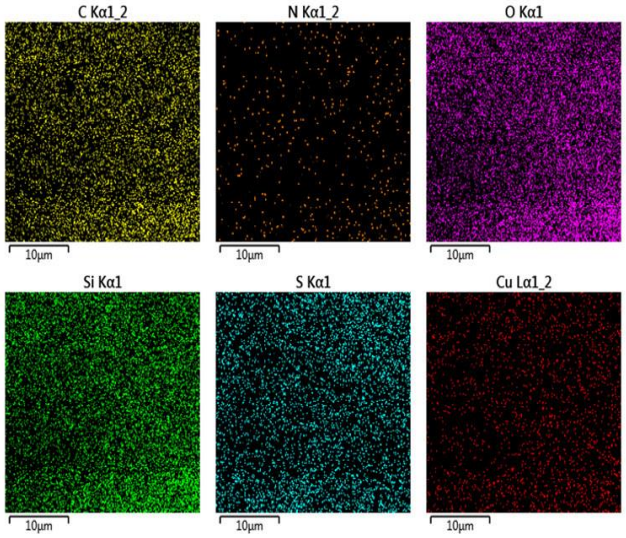

Figure 4. Elemental mapping of CuS@mSiO$_2$-SB-Cu.

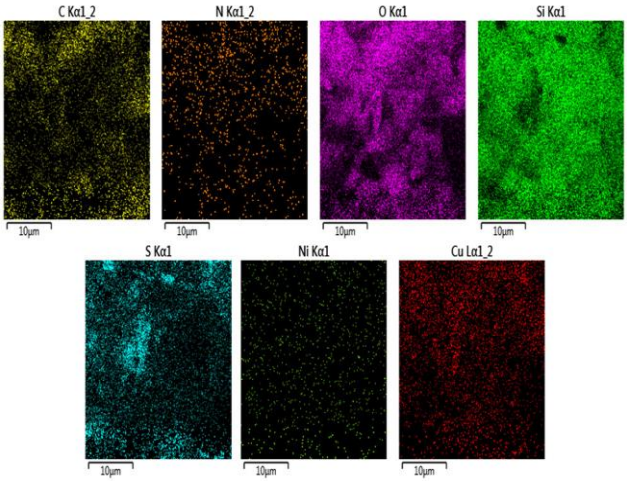

Figure 5. Elemental mapping of CuS@mSiO$_2$-SB-Ni.

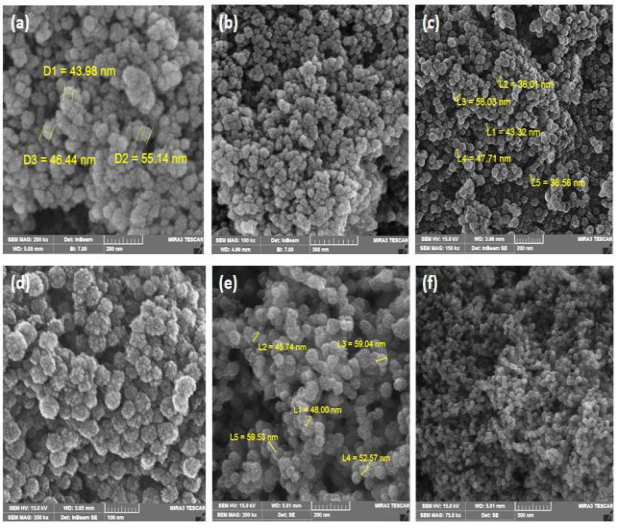

Figure 6. FE-SEM images of the nanoparticles: (a, b) CuS@mSiO$_2$, (c, d) CuS@mSiO$_2$-SB-Cu and (e, f) CuS@mSiO$_2$-SB-Ni.

in Figure 8. In the XRD pattern of CuS@mSiO$_2$, a single intense peak at 2θ = 1.98 is assigned to reflection from the (1 0 0) plane and is characteristic of the ordered hexagonal mesoporous structure.[19,23,33-35] The broadening of this peak in XRD pattern of CuS@mSiO$_2$-SB-Cu and CuS@mSiO$_2$-SB-Ni is related to decreasing of the regularity of mesostructure due to functionalization.[19, 21, 36] A broad peak about 2θ = 4 in XRD pattern of CuS@mSiO$_2$ is attributed to reflections from the (1 1 0) and (2 0 0) planes. This peak was disappeared after functionalization.

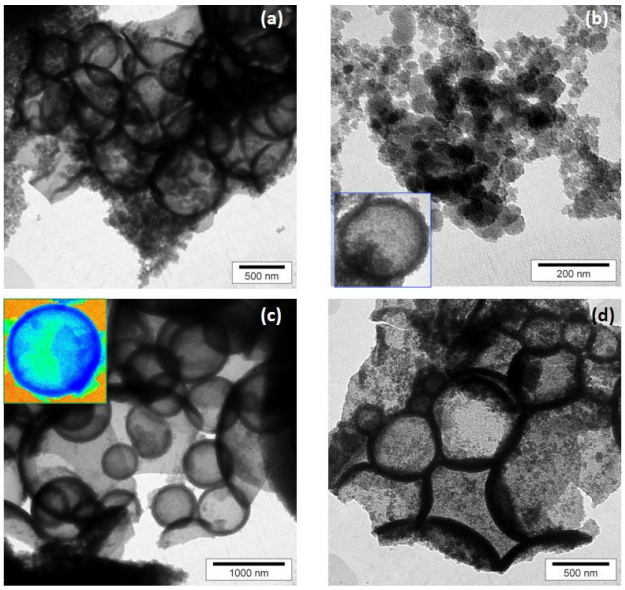

Figure 7. TEM images of (a,b) CuS@mSiO$_2$, (c,d) CuS@mSiO$_2$-SB-Ni.

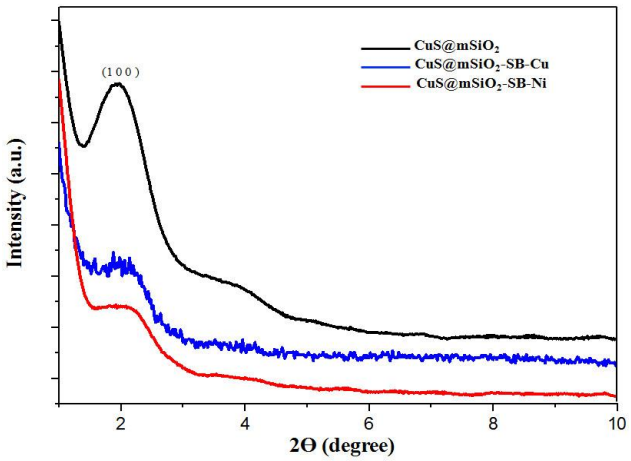

Figure 8. Low angle X-ray diffraction patterns of CuS@mSiO$_2$, CuS@mSiO$_2$-SB-Cu and CuS@mSiO$_2$-SB-Ni.

Figure 9 shows the nitrogen adsorption-desorption isotherms of CuS@mSiO$_2$, CuS@mSiO$_2$-SB-Cu and CuS@mSiO$_2$-SB-Ni. The BET and BJH data are compared in the Table 1. These isotherms correspond to compared in the Table 1. These isotherms correspond to

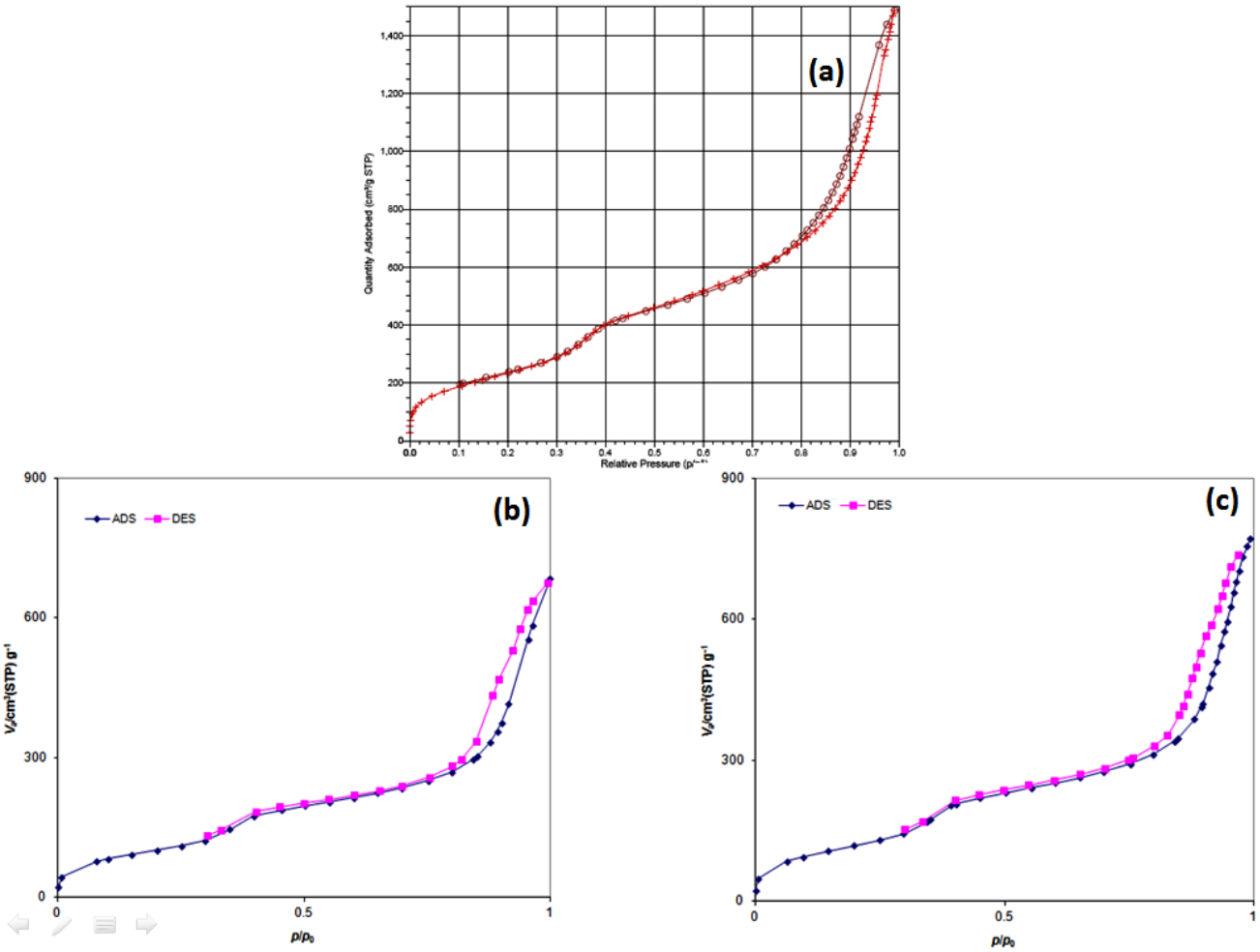

Figure 9. N_2 adsorption-desorption isotherms of (a) CuS@mSiO$_2$, (b) CuS@mSiO$_2$-SB-Cu and (c) CuS@mSiO$_2$-SB-Ni.

Table 1. BET and BJH data of CuS@mSiO$_2$, CuS@mSiO$_2$-SB-Cu and CuS@mSiO$_2$-SB-Ni

Sample	BET surface area ($m^2\ g^{-1}$)	Pore volume ($cm^3\ g^{-1}$)	Pore size (nm)
CuS@mSiO$_2$	920.00	2.33	7.78
CuS@mSiO$_2$-SB-Cu	482.52	1.01	8.43
CuS@mSiO$_2$-SB-Ni	579.04	1.18	8.18

the type IV isotherm and a hysteresis at relative pressures P/P_o of 0.45-0.9 is the characteristic of mesoporous materials based on the IUPAC classification. On the basis of BET and BJH data surface area, pore volume and pore size for CuS@mSiO$_2$ are 920.00 m^2/g, 2.33 cm^3/g and 7.78 nm, respectively. After the grafting of metal complex, the surface area and pore volume are obviously reduced because the functionalization causes the pores to be blocked and the porosity to decrease.[20,22,36,37]

Thermogravimetric analysis (TGA) curves of CuS@mSiO$_2$-SB-Cu and CuS@mSiO$_2$-SB-Ni are presented in Fig. 10. The first weight loss below 200 °C is related to the removal of physically adsorbed water or solvent on the surface or inside the pores of silica.[22,23,38]

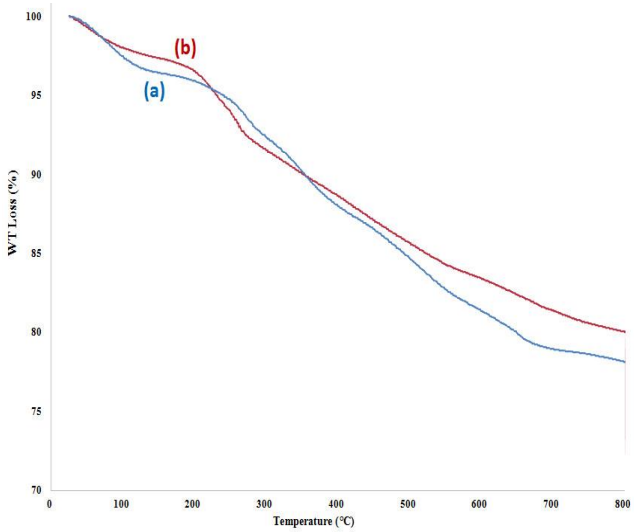

Figure. 10 The TGA curve of the (a) CuS@mSiO$_2$-SB-Cu and (b) CuS@mSiO$_2$-SB-Ni.

The second weight loss (17-18%) in the temperature range of 200-800 °C corresponds to the degradation of

organic materials.[21,39] The residue is related to inorganic moieties.

Assessment of the antibacterial activity and antibiotic loading

Three antibiotics, streptomycin, gentamycin and polymyxin, were loaded on the CuS@mSiO$_2$, CuS@mSiO$_2$-SB, CuS@mSiO$_2$-SB-Cu and CuS@mSiO$_2$-SB-Ni and their antibacterial activity along with primary nanocomposites were evaluated by recording the absorbance of bacterial culture at 655 nm. Figures S1-S24 show the growth curves of treated bacteria and Table 2 gives the MIC and MBC data. The results reveal that antibiotic loaded nanocomposites affect both gram-positive and gram-negative bacteria, but nanocomposites without antibiotic have little or no effect. It was also found that both CuS@mSiO$_2$ and functionalized CuS@mSiO$_2$ are able to carry antibiotics because of their porous structure, but functionalized CuS@mSiO$_2$ due to having silanol groups, pendant functional groups and metal centers are more suitable for interaction with antibiotic functional groups. The results of MIC and MBC for antibiotic loaded composites (Table 2) show that CuS@MCM-41-Gen compared to CuS@MCM-41-Str and CuS@MCM-41-Pol has the ability to inhibit *P.aeruginosa* at a lower concentration, while the minimum concentration required to inhibit *S. aureus* is the same for all three. Antibiotic loaded CuS@mSiO$_2$-SB, CuS@mSiO$_2$-SB-Cu and CuS@mSiO$_2$-SB-Ni show low MIC and MBC values against S. *aureus* and all of them have bactericidal properties. These nanoparticles also indicate inhibitory effects against *P.aeruginosa* in low concentrations and bactericidal properties at higher concentrations.

Table 2. MIC and MBC data for synthesized nanocomposites against *P.aeruginosa* and *S. aureus* bacteria

Sample	*P.aeruginosa*		*S. aureus*	
	MIC (mg/mL)	MBC (mg/mL)	MIC (mg/mL)	MBC (mg/mL)
CuS@mSiO$_2$-Str	1	1	1	2
CuS@mSiO$_2$-Gen	0.5	2	1	2
CuS@mSiO$_2$-Pol	2	2	1	1
CuS@mSiO$_2$-SB-Str	0.5	4	1	2
CuS@mSiO$_2$-SB-Gen	0.5	2	0.5	0.5
CuS@mSiO$_2$-SB-Pol	0.5	2	0.5	0.5
CuS@mSiO$_2$-SB-Ni-Str	0.5	4	0.5	0.5
CuS@mSiO$_2$-SB-Ni-Gen	0.5	1	0.5	0.5
CuS@mSiO$_2$-SB-Ni-Pol	0.5	4	0.5	0.5
CuS@mSiO$_2$-SB-Cu-Str	0.5	1	0.5	0.5
CuS@mSiO$_2$-SB-Cu-Gen	0.5	2	0.5	0.5
CuS@mSiO$_2$-SB-Cu-Pol	0.5	1	0.5	0.5

DNA damage studies

DNA cleavage activity of nanocomposites was investigated by agarose gel electrophoresis method. Figure 11 represents the electrophotogram for the cleavage activity of CuS@mSiO$_2$, CuS@mSiO$_2$-SB, CuS@mSiO$_2$-SB-Cu and CuS@mSiO$_2$-SB-Ni on the isolated DNA of S. *aureus* and *P. aeruginosa* compared to the control DNA of bacteria. The results show that all nanocomposires have considerable destructive effects on isolated DNA of bacteria, because the agerose well is darkened. Therefore DNA cleavage activity may be a bactericidal mechanism for these nanoparticles.

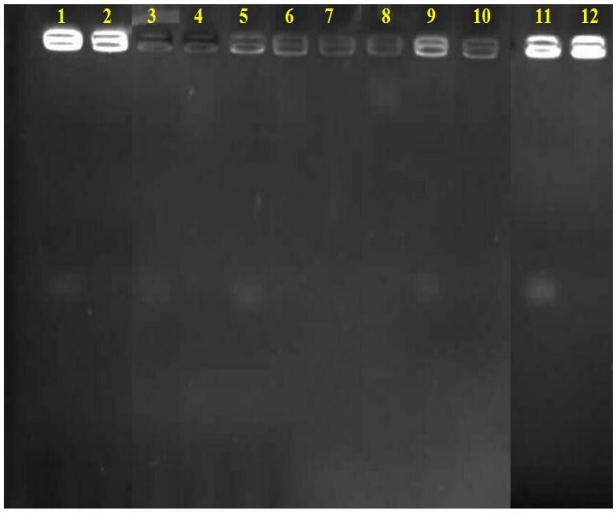

Figure 11. The electrophotogram for the DNA cleavage activity of the nanocomposites. **1** = unreacted DNA of *S. aureus*, **2** = unreacted DNA of *P. aeruginosa*, **3** = CuS@mSiO$_2$ + *S. aureus* DNA, **4** = CuS@mSiO$_2$ + *P. aeruginosa* DNA, **5** = CuS@mSiO$_2$-SB + *S. aureus* DNA, **6** = CuS@mSiO$_2$-SB + *P. aeruginosa* DNA, 7 = CuS@mSiO$_2$-SB-Ni + *S. aureus* DNA, **8** = CuS@mSiO$_2$-SB-Ni + *P. aeruginosa* DNA, **9** = CuS@mSiO$_2$-SB-Cu + *S. aureus* DNA, **10** = CuS@mSiO$_2$-SB-Cu + *P. aeruginosa* DNA, **11** = *S. aureus* DNA + H_2O_2, **12** = *P. aeruginosa* DNA + H_2O_2.

Enzyme immobilization

In order to find the potential of synthesized composites for binding to enzymes, immobilization of α-amylase enzyme was examined. The results of enzyme immobilization on CuS@mSiO$_2$, CuS@mSiO$_2$-SB, CuS@mSiO$_2$-SB-Cu and CuS@mSiO$_2$-SB-Ni are shown in Fig. 12 and listed in Table 3. As indicated by the diameter of the starch hydrolysis zone, α-Amylase was successfully immobilized on all compounds. Among these, functionalized nanocomposites, CuS@mSiO$_2$-SB, CuS@mSiO$_2$-SB-Cu and CuS@mSiO$_2$-SB-Ni, loaded the enzyme more efficiently than CuS@mSiO$_2$. Schiff base and metal complexes on mesoporous silicates provide OH and C=N groups or free coordination sites suitable for interaction with amine groups of amylase. So these functionalized CuS@mSiO$_2$ nanoparticles are good candidates for enzyme immobilization.

Table 3. Starch hydrolysis zone diameter (mm) around composites

Samples	Effect zone (mm)
CuS@mSiO$_2$	24
CuS@mSiO$_2$-SB	31
CuS@mSiO$_2$-SB-Cu	27
CuS@mSiO$_2$-SB-Ni	36

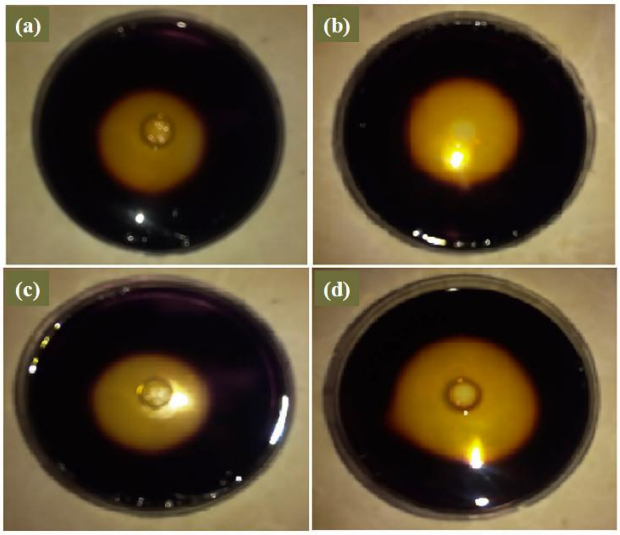

Figure 12. Starch hydrolysis zone diameter (mm) following the effect of enzyme conjugated (a) $CuS@mSiO_2$, (b) $CuS@mSiO_2$-SB, (c) $CuS@mSiO_2$-SB-Cu and (d) $CuS@mSiO_2$-SB-Ni.

4. CONCLUSION

$CuS@mSiO_2$ core-shell nanoparticles were functionalized by Cu(II) and Ni(II) Schiff base complexes and fully characterized. These organic-inorganic hybrid nanomaterials were found to be a good nano-network for loading of streptomycin, gentamycin and polymyxin and can be regarded as a carrier for drug delivery systems to fight against bacterial species. Results of enzyme immobilization revealed that functionalized $CuS@mSiO_2$ nanoparticles efficiently immobilize α-amylase and retain its stability and functional efficiency. Therefore, these nanomaterials can be potentially used as biocatalysts. Also the results showed that the DNA cleavage can be a mechanism for antibacterial activities of synthesized nanocomposites

CONFLICTS OF INTEREST

There is no conflict of interest to declare.

ACKNOWLEDGMENTS

Support of this work by Shahid Chamran University of Ahvaz, Ahvaz, Iran (Grant No. SCU.SC99.835) is gratefully acknowledged.

Supplementary material

The effect of synthesized nanomaterials on growth curve of bacteria has been given in Figures S1-S24.

AUTHOR INFORMATION

Corresponding Author

Tahereh Sedaghat: Email: tsedaghat@scu.ac.ir, *ORCID: 0000-0002-3352-1932*

Author(s)

Ameneh Ahmadi, Hossein Motamedi

REFERENCES

1. A. Farrokhi, M. Asaadzadeh, F. Feizpour, *Inorg. Chem. Res.* **2021**, *5*, 1-9.
2. H. Furukawa, K.E. Cordova, M. O'Keeffe, O.M. Yaghi, *Science* **2013**, *341*, 123044.
3. M. Zendehdel, M. Haddadi, Z. Mortezaei, *Inorg. Chem. Res.* **2021**, *5*, 193-200.
4. Y. Li, H. Cao, J. Yu, *Acs Nano* **2018**, *12*, 4096-4104.
5. V. Malgras, J. Tang, J. Wang, J. Kim, N.L. Torad, S. Dutta, K. Ariga, M. Hossain, A. Shahriar, Y. Yamauchi, *J. Nanosci. Nanotechnol.* **2019**, *19*, 3673-3685.
6. T. Juarez, J. Biener, J. Weissmüller, A.M. Hodge, *Adv. Eng. Mater.* **2017**, *19*, 1700389.
7. R. Zhang, M. Hua, H. Liu, J. Li, *Mater. Sci. Eng. B Solid State Mater. Adv. Technol.* **2021**, *263*, 114835.
8. R. Sacourbaravi, Z. Ansari-Asl, M. Kooti, V. Nobakht, *Inorg. Chem. Res.* **2021**, *5*, 112-119.
9. Z. ALOthman, *Materials* **2012**, *5*, 2874-2902.
10. R.K. Kankala, Y.H. Han, J. Na, C.H. Lee, Z. Sun, S.B. Wang, T. Kimura, Y.S. Ok, Y. Yamauchi, A.Z. Chen, *Adv. Mater.* **2020**, *32*, 1907035.
11. R. Narayan, U.Y. Nayak, A.M. Raichur, S. Garg, *Pharmaceutics* **2018**, *10*, 118.
12. V.-C. Niculescu, *Front. Mater. Sci* **2020**, *7*, 36.
13. H. Ahmed, S.S. Gomte, E. Prathyusha, P.A.M. Agrawal, A. Alexander, *J. Drug Deliv. Sci. Technol.* **2022**, *76*, 103729.
14. T.T.H. Thi, T.N.Q. Nguyen, D.T. Hoang, D.H. Nguyen, *Mater. Sci. Eng. C* . **2019**, *99*, 631-656.
15. H. Li, X. Chen, D. Shen, F. Wu, R. Pleixats, J. Pan, *Nanoscale* **2021**, *13*, 15998-16016.
16. Z. Zhou, M. Hartmann, *Chem. Soc. Rev.* **2013**, *42*, 3894-3912.
17. E. Magner, *Chem. Soc. Rev.* **2013**, *42*, 6213-6222.
18. A.M. Sulman, A.K. Haskell, B.B. Tikhonov, O.V. Grebennikova, A.I. Sidorov, L.M. Bronstein, V.G. Matveeva, *Microporous Mesoporous Mater.* **2022**, *341*, 112092.
19. M. Jalalzadeh-Esfahani, T. Sedaghat, A. Beheshti, R. Azadi, *J. Porous Mater.* **2022**, 29, 1149-1164.
20. A. Ahmadi, T. Sedaghat, R. Azadi, H. Motamedi, *Catal. Lett.* **2020**, *150*, 112-126.
21. A. Ahmadi, T. Sedaghat, H. Motamedi, R. Azadi, *Appl. Organomet. Chem.* **2020**, *34*, e5572.
22. A. Ahmadi, T. Sedaghat, R. Azadi, *J. Inorg. Organomet. Polym. Mater.* **2021**, *31*, 4126-4140.
23. L. Tahmasbi, T. Sedaghat, H. Motamedi, M. Kooti, *J. Solid State Chem.* **2018**, *258*, 517-525.
24. J. Chen, C. Ning, Z. Zhou, P. Yu, Y. Zhu, G. Tan, C. Mao, *Prog. Mater. Sci.* **2019**, *99*, 1-26.
25. L. Wang, *RSC Adv.* **2016**, *6*, 82596-82615.

26. J. Wang, X. Wu, P. Shen, J. Wang, Y. Shen, Y. Shen, T.J. Webster, J. Deng, *Int. J. Nanomedicine* **2020**, *15*, 1903.
27. P. Geng, N. Yu, D.K. Macharia, R. Meng, P. Qiu, C. Tao, M. Li, H. Zhang, Z. Chen, W. Lian, *Chem. Eng. J.* **2022**, *441*, 135964.
28. X. Liu, Q. Ren, F. Fu, R. Zou, Q. Wang, G. Xin, Z. Xiao, X. Huang, Q. Liu, J. Hu, *Dalton Trans.* **2015**, *44*, 10343-10351.
29. J. Sambrook, E.F. Fritsch, T. Maniatis, Molecular cloning, Cold spring harbor laboratory press New York, **1989**.
30. T. Sedaghat, Y. Ebrahimi, L. Carlucci, D.M. Proserpio, V. Nobakht, H. Motamedi, M.R. Dayer, *J. Organomet. Chem.* **2015**, *794*, 223-230.
31. L. Zhang, Z. Yang, W. Zhu, Z. Ye, Y. Yu, Z. Xu, J. Ren, P. Li, *ACS Biomater. Sci. Eng.* **2017**, *3*, 1690-1701.
32. Y. Wang, B. Li, L. Zhang, P. Li, L. Wang, J. Zhang, *Langmuir* **2012**, *28*, 1657-1662.
33. L. Yuan, W. Chen, J. Hu, J.Z. Zhang, D. Yang, *Langmuir* **2013**, *29*, 734-743.
34. L. Yuan, Q. Tang, D. Yang, J.Z. Zhang, F. Zhang, J. Hu, *J. Phys. Chem. C* **2011**, *115*, 9926-9932.
35. F. Carniato, C. Bisio, G. Paul, G. Gatti, L. Bertinetti, S. Coluccia, L. Marchese, *J. Mater. Chem.* **2010**, *20*, 5504-5509.
36. D. Zhang, X. Wang, Z.-a. Qiao, D. Tang, Y. Liu, Q. Huo, *J. Phys. Chem. C* **2010**, *114*, 12505-12510.
37. D. Tang, L. Zhang, Y. Zhang, Z.-A. Qiao, Y. Liu, Q. Huo, *J. Colloid Interface Sci.* **2012**, *369*, 338-343.
38. C.-C. Liu, T.-S. Lin, S.I. Chan, C.-Y. Mou, *J. Catal.* **2015**, *322*, 139-151.
39. M. Rajabzadeh, H. Eshghi, R. Khalifeh, M. Bakavoli, *RSC Adv.* **2016**, *6*, 19331-19340.